Phonons in layered compounds

2001 J. Phys.: Condens. Matter 13 7679

(http://iopscience.iop.org/0953-8984/13/34/313)

INSTITUTE OF PHYSICS PUBLISHING JOURNAL OF PHYSICS: CONDENSED MATTER

J. Phys.: Condens. Matter **13** (2001) 7679–7690 PII: S0953-8984(01)24208-8

Phonons in layered compounds

Hartmut Zabel

Institut für Experimentalphysik/Festkörperphysik, Ruhr-Universität Bochum, D-44780 Bochum, Germany

E-mail: hartmut.zabel@ruhr-uni-bochum.de

Received 24 April 2001
Published 9 August 2001
Online at stacks.iop.org/JPhysCM/13/7679

Abstract

Layer compounds exhibit highly anisotropic structural and elastic properties. They are characterized by rather rigid layers, loosely stacked together perpendicular to each other. Accordingly, the phonon dispersion of layered compounds are characterized by low lying *inter*-layer modes and high-frequency *intra*-layer modes. Intercalation compounds composed of a regular sequence of host and guest layers provide a playground for the investigation of the layer lattice dynamics by systematically changing the guest species and the number of guest layers per unit cell. In this contribution a brief overview of some characteristic features of the lattice dynamics of layered compounds is provided.

1. Introduction

Layer compounds exhibit highly anisotropic structural and elastic properties. They are characterized by rather rigid layers, loosely stacked together perpendicular to each other. Layered compounds can quite frequently be found in nature in form of clays or graphite materials. Also sulfide, selenide and telluride compounds together with transition metals form layered compounds, such as MoS_2, TaS_2 or GeSe. In a broader sense copper oxide compounds with high-temperature superconductivity also belong to this class of material. Layered compounds often can be intercalated with other chemical species of molecules, forming layered intercalation compounds. Graphite and its numerous intercalation compounds may be the best known layered guest–host system. For a general review of these compounds the reader is referred to [1]. In figure 1 the schematics of layered compounds and the different possibilities for intercalation of the host layers are displayed. In the first class the host consists of monolayers and the number of host layers (n) between any consecutive intercalate layer characterizes the stage n of the compound. In the second class the host layer consists of a triple layer usually forming only a stage 1 compound. In the third class the host layers have a complex internal architecture, and after intercalation to a stage 1 compound the number of intercalated layers per gap can be varied.

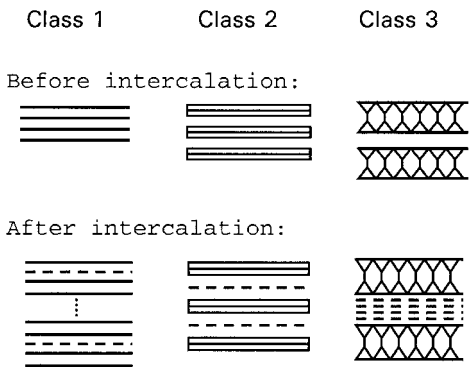

Figure 1. Schematic diagrams of the various classes of layered compounds before and after intercalation. Before intercalation the compound may consist of single layers, or a stack of several layers, in some cases with complex internal structure. After intercalation several different stages may form in case of the class 1 compounds, where the stage n is defined as the number of host layers between any consecutive intercalate layers. The class 2 compounds form only stage 1 compounds. In the class 3 compounds several guest layers may intercalate within any particular gap of the host system.

Graphite and, in particular, graphite intercalation compounds (GICs) with a regular sequence of alternating intercalate layers and graphite basal planes (also termed 'graphene layers') belong to the first class of intercalation compounds. They represent a unique laboratory for the exploration of phonons in layered materials. By changing the intercalate species, the stage of the compound, or the intercalate in-plane stoichiometry, the symmetry and interaction can be altered in a systematic fashion, allowing detailed investigations of the relation between structure and phonons. In addition, the intercalated layers in graphite display a rich variety of ordered and disordered structures, commensurate and incommensurate phases, melting transitions on periodic substrates, and metal–insulator transitions. In all these cases examination of the lattice dynamics is of prime interest for obtaining interatomic potentials, which, in turn, leads to an accurate modelling of the structures, dynamics, and phase transitions in these compounds.

2. Basic concepts of layer lattice dynamics

The lattice dynamics of layered compounds can be classified as high-frequency *intra*-layer modes and low-frequency *inter*-layer modes. The different eigenmodes are schematically sketched in figure 2 for the case of GICs. The energy separation between the inter- and intralayer modes is a measure for the elastic anisotropy of the material. In addition we find modes specific to the intercalate atoms or molecules. These comprise either simple in-plane longitudinal and transverse modes in the case of monoatomic intercalate layers or more complex intra-molecular modes in the case of molecular intercalates.

In figure 3 the dispersion of the low lying modes is sketched within an energy regime accessible to inelastic neutron scattering work. These modes comprise the acoustic and optic branches of the [00q] longitudinal modes (L) ('layer breathing modes') and the [00q] transverse modes (T) or 'layer shear modes'. Both modes propagate perpendicular to the graphite and intercalate layers. The layered structure of the compounds leads, in addition, to very soft [q00]T modes, which propagate parallel to the layers with polarization perpendicular to the graphene and intercalate planes. These modes are commonly referred to as 'layer bending' or

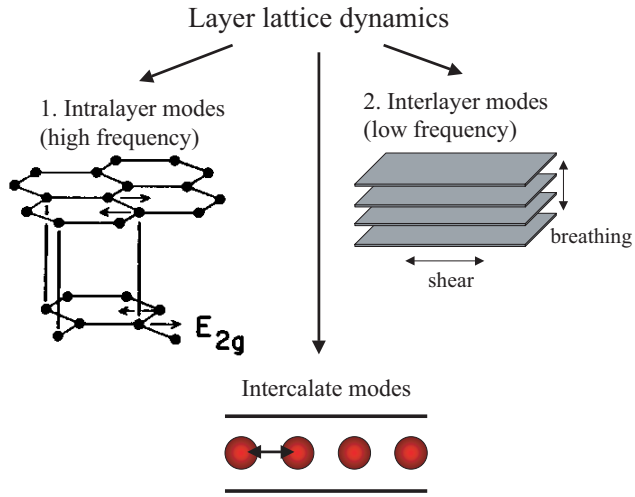

Figure 2. Schematic diagram of the layer lattice dynamics of GICs. The lattice dynamics is characterized by high-frequency intralayer modes and low-frequency interlayer modes. The latter modes separate in layer breathing, layer shear and bending modes, as shown in figure 3. In addition, after intercalation intercalate modes may appear, which are characteristic for the intercalate species.

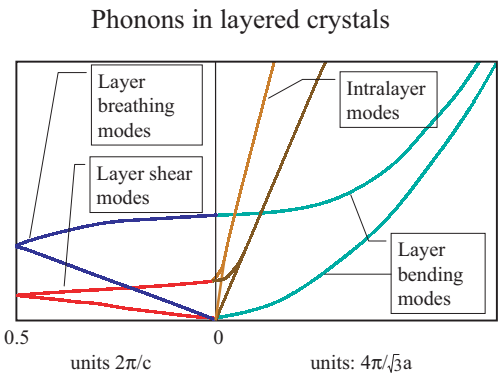

Figure 3. The phonon dispersion of the low lying modes in GICs and other layered compounds is schematically shown. The layered nature of the compounds and the high elastic anisotropy can be immediately recognized by the presence of layer bending modes with quadratic dispersion.

'ripple' modes.

The full exploration of the lattice dynamics of GICs via inelastic neutron scattering is hampered by the lack of sufficiently large single crystals. Therefore, all phonon data from neutron scattering are derived from highly oriented pyrolytic graphite (HOPG) materials. HOPG is a textured material with a c-axis mosaicity 0.2–3°, depending on the quality of the material, and a completely random in-plane orientation. The two-dimensional powder nature of this material has no effect on the [00q]L phonons which propagate along the oriented c-axis. In fact, the [00q]L modes are the most frequently measured phonon modes of GICs. The [q00]T modes are also rather well defined in spite of the powder average ($HK0$) plane, owing to the close elastic isotropy of the graphite and intercalate planes. All other modes are more difficult to determine and have been measured only in a few cases. For further information

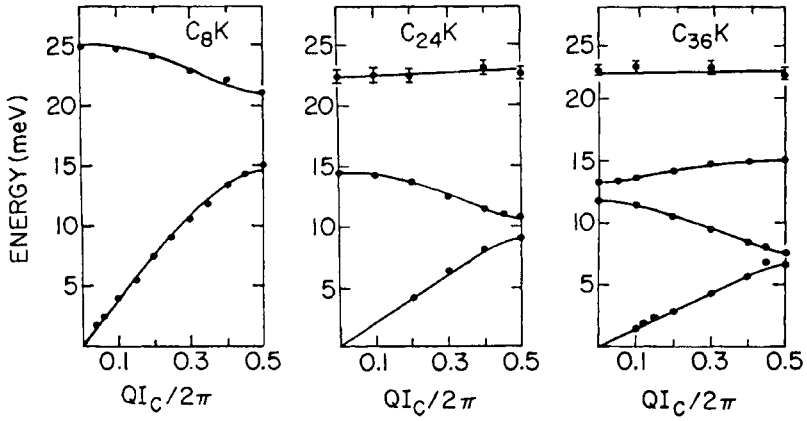

Figure 4. Measured phonon energies of [00q]L modes in KC_n alkali-metal GICs at room temperature. The full curves represent best fits to the phonon energies with one-dimensional lattice dynamical models described in the text (from [3]).

and historical remarks the reader is referred to a more detailed review paper on this subject in [2].

3. Layer breathing or [00q]L modes

3.1. The effect of staging

The effect of staging on the phonon dispersion of the [00q]L modes is clearly seen by the sequence of potassium-GICs from stage 1 to 3, whose phonon energies are reproduced in figure 4 [3]. An increase of the stage number by one results in the appearance of an additional optic branch. For all stages, zone folding and mode splitting effects are clearly visible. The highest optic branch is predominantly determined by the vibrational amplitude of the planes with the smallest effective mass. These are the potassium layers in all three K-GICs. It should be noted that with increasing stage number the dispersion of the top optic branch becomes flatter, indicating that the coupling between the alkali-metal planes weakens from stage 1 to 3. This will be discussed in more detail below.

The [00q]L phonon dispersion of GICs can be described as the dispersion of linear chains of mass points, representing the graphene and intercalate layers. Therefore, the dispersion depends on the areal mass densities of the intercalate layers, the force constants between the layers and the number of layers within a repeat unit. For the case of alkali-metal GICs, a stage n compounds contains $n + 1$ layers, n graphene layers between consecutive intercalate layers and one intercalate layer. Then the dispersion consists of $n + 1$ phonon branches, one acoustic branch and n optic branches. The full curves in figure 4 are fits to the data points with a very simple Born–von Karman (BvK) lattice dynamical model taking into account the graphite mass M_C in atomic mass units ($M_C = 12$ au), the intercalate effective mass per layer and per carbon atom: $M_{eff} = M_K/x$, where M_K is in atomic units and x is the layer stoichiometry, a force constant ϕ_I connecting the intercalate and the bounding graphene layers and a force constant ϕ_C for the inner graphene layers. The fit can be dramatically improved by introducing a third force constant ϕ', connecting the graphene layers across an intercalate layers [4]. An alternative mixed ion–shell and BvK model was proposed to account for the charge transfer and the ionic character of the intercalate layers [3, 5]. In this model the interaction between

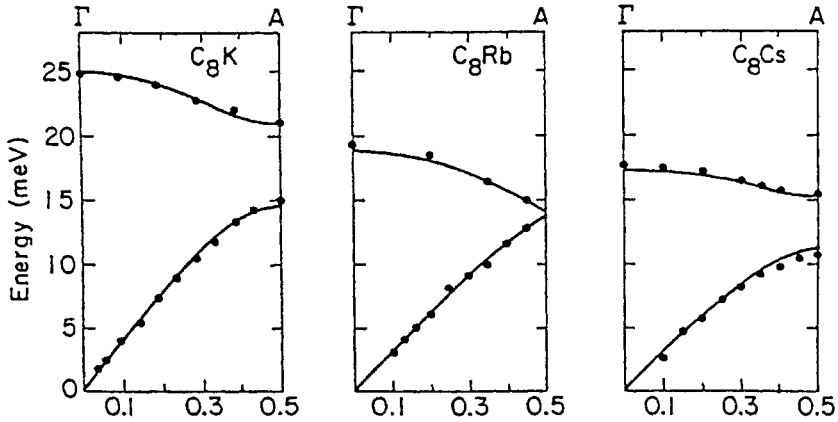

Figure 5. The effective mass of the intercalate layer determines the dispersion of the optical branch of the $[00q]$L modes in the stage 1 compounds of KC_8, RbC_8 and CsC_8. The effective mass of the potassium intercalate plane is lighter than the graphene plane, explaining the high optic branch and the large gap at the zone boundary. The effective mass of the rubidium intercalate layer is almost identical to that of graphene, while the effective mass of the cesium intercalate layer is heavier than the graphene layer (from [3]).

the intercalate and bounding graphene layers is mediated by an electronic shell whose mass is assumed to be zero. The shell is coupled to the core of the alkali-metal ion by a force constant ϕ_K and to the bounding graphite layers by the shell force constant ϕ_S.

3.2. The effect of intercalate mass

The effect of the intercalate mass on the phonon energies is best demonstrated by the series of stage 1 compounds KC_8, RbC_8 and CsC_8, the phonon dispersions of which are reproduced in figure 5. For all three compounds the symmetry along the c-axis and the number ratio of intercalate to carbon atoms is the same, and there are only small differences in the force constants. The dominant effect is attributable to the in-plane effective mass of the intercalate layer. In KC_8, with the lightest intercalate mass, the optic branch is well separated from the acoustic branch by a large frequency gap. The Rb intercalate layer has an effective mass which is only slightly smaller than that of the graphene plane. Therefore the mode splitting at the Brillouin zone boundary is only marginal. Finally, in CsC_8 the Cs layer is heavier than the graphene layer, reversing the role of vibrating planes at the Brillouin zone boundary.

3.3. Localized modes

The Einstein-like behaviour of the top optic mode in high stage compounds can be modelled assuming a single alkali-metal layer intercalated in an otherwise pure graphite crystal. Coupling this layer to the adjacent graphene layers by a force constant ϕ_I, and the graphite layers via the usual force constant ϕ_C, this simple model predicts a vibrational amplitude of the defect mode which is exponentially damped proportional to the mass difference ΔM between the intercalate and graphite layers. Figure 6 shows the vibrational amplitude for isolated K, Rb and Cs layers in graphite as a function of the number of graphite planes s away from the intercalate layer. Due to the large mass mismatch, the K vibrational amplitude is most strongly attenuated and the wavefunction of the localized mode does not extend much further than one graphite layer from its origin. This explains the weak dispersion of the K optic branch in the

stage 3 K-GIC. On the other hand, the Cs layers in compounds with $n \geqslant 2$ have an effective mass of 11.08 au, which is closely matched to M_C. Therefore, the local vibration can propagate over several graphite planes. Consequently, the top optic branch of CsC_{36} should exhibit more dispersion, which is indeed the case [4].

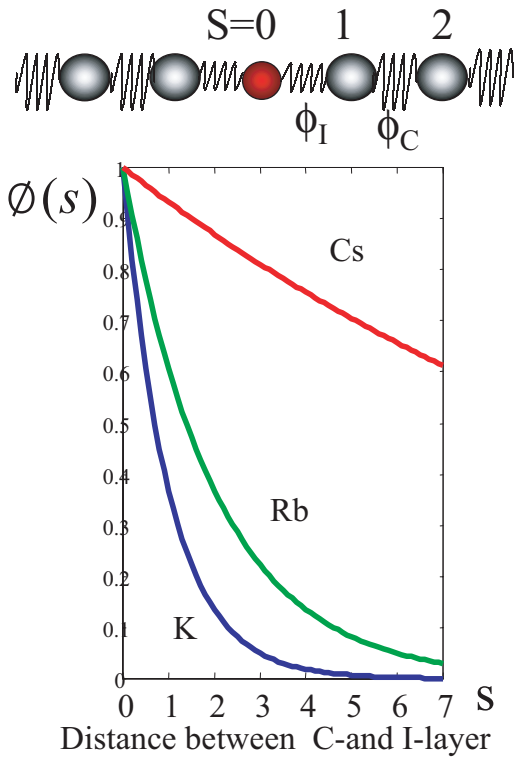

Figure 6. Amplitude of longitudinal vibrations of isolated intercalate layers in graphite against the number of graphite layers away from the intercalates at the origin.

4. [q00]T phonon dispersion

One of the most intriguing features of layered compounds are the [q00]T modes with a parabolic dispersion relation at small phonon wavenumbers: $\omega \propto q^2$. These phonon modes are fingerprints for the layered nature of the compound in question with weak interlayer shear interaction. They are characteristic of the bending of single isolated sheets of homogeneous material and are therefore referred to as bending modes or ripple modes. Increasing the shear interaction between neighbouring layers causes the dispersion to have a non-zero slope at $q = 0$. Therefore the dispersion for small q can be written

$$\omega^2 = Aq^2 + Bq^4. \tag{1}$$

The slope $A^{1/2}$ at $q = 0$ is given by $(C_{44}/\rho)^{1/2}$, where C_{44} is the layer shear elastic constant and ρ is the volume density. This is the same elastic constant as determines the slope of the acoustic [00q]T branch. While it is very difficult to measure, by inelastic neutron scattering, the extremely soft [00q]T modes, the analysis of the bending modes also yields information

on the layer shear interaction. B is the parameter determining the resistance of the layer to bending, referred to as the 'bending stiffness constant'. Both parameters, B and C_{44}, can be obtained from the acoustic dispersion relation by plotting ω^2/q^2 as a function of q^2. Since all experimental data on $[q00]$T modes in GICs were obtained using intercalated HOPG material, constant Q scans are not capable of distinguishing between phonons propagating along the [100] or [110] directions. However, owing to the relative elastic isotropy of the graphite and intercalate planes, no essential difference for both directions is expected. Early measurements of layer bending modes have been carried out on pristine graphite by Nicklow *et al* [6] and subsequently on some transition-metal dichalcogenides, in particular on 2H-MoS_2 by Wakabayashi and Nicklow [7]. However, only the GICs with the large variety of intercalates and stages allow a systematic exploration of these modes and their dependence on phase transitions and charge transfer effects.

The $[q00]$T modes in donor compounds have been investigated by a number of authors [8, 9]. Experimental results from room-temperature measurements of stage 1 compounds are shown in figure 7. In all cases the quadratic dispersion of the acoustic branch is clearly visible. While the dispersion of the acoustic branch is determined by the bending stiffness constant of the combined graphite and intercalate layers, the dispersion of the optic branches is sensitive to the bending modulus of the individual layers. Analysis of the bending modes show that in GICs the bending stiffness constant is dominated by the graphene layers, whereas the alkali-metal intercalate layers are rather 'floppy'.

5. Phonon density of states of intercalate modes

For most of the phonon modes discussed so far, the intercalate and host graphite displacements are coupled. This is the case to a much lesser extent for the intercalate in-plane modes with propagation and polarization parallel to the planes. In the plane, the extremely strong C–C interaction leads to $[q00]$T and $[q00]$L dispersions with very steep slopes (see figure 3). The bonds between the intercalate atoms or molecules are usually much weaker and their vibration is therefore essentially decoupled from the graphite modes. Because of the lack of single crystals, the dispersion of the intercalate in-plane modes is difficult to measure. It is therefore better practice to determine both the longitudinal and transverse modes via phonon-density-of-state (PDS) measurements. In general, PDSs are obtained via incoherent mixing and averaging of phonon modes, usually achieved using nuclei with predominant incoherent scattering cross sections for thermal neutron scattering. For alkali-metal intercalate atoms the scattering lengths are, however, exclusively coherent, The same effect of incoherent mixing is then achieved by adding and averaging the coherent phonon signal over many Brillouin zones. This procedure is termed the 'incoherent approximation' [10]. In case of GICs and because of the large disparity between the graphite and intercalate vibrational frequencies, partial PDSs of the intercalate modes with propagation and polarization parallel to the layers are obtained:

$$S(Q, \nu) = \frac{\alpha Q^2 \sigma}{M_I \nu}[n(\nu) + 1]\mathrm{e}^{-2W_I} g(\nu) + L(Q, \nu). \tag{2}$$

Here $n(\nu)$ is the Bose–Einstein occupation number; M_I and σ are the mass and the cross section of the intercalate species, respectively; α is a constant; W_I is the Debye–Waller factor for the intercalate in-plane vibration; and $\nu = 2\pi/\omega$ is the vibrational frequency. The first term in the above equation represents the one-phonon dynamical scattering function, from which the PDSs $g(\nu)$ can be calculated. The second term, $L(Q, \nu)$, collects all contributions from multiphonon processes, which is usually a smooth function of ν and not easily distinguished

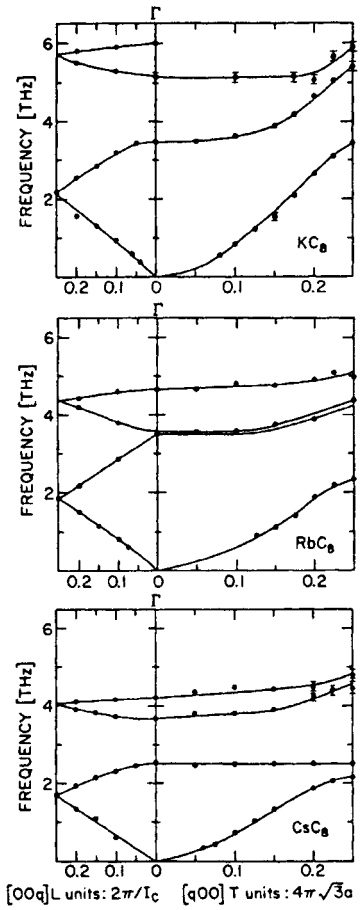

Figure 7. Measured phonon dispersions of [q00]T modes in stage 1 alkali-metal GICs. The left-hand panels reproduce the [00q]L modes and the right-hand panels show the bending modes. The figure was compiled from the following references: KC_8 and CsC_8 from [9] and RbC_8 from [8].

from a uniform background. Nonetheless, the PDS data shown below have been corrected for two-phonon contributions and for graphite contributions via procedures described in [11].

The PDS of a two-dimensional lattice is expected to increase linearly with ν at small frequencies ($g(\nu) \propto \nu$) and should exhibit two peaks at larger frequencies from the flat parts of the transverse and longitudinal dispersion close to the Brillouin zone boundary. Turning on the substrate potential causes a gap to occur in the PDS of the size $\nu_0 = (1/2\pi)(\phi_{IC}/M_I)^{1/2}$, where ϕ_{IC} represents the intercalate–graphite in-plane coupling constant, which is proportional to the curvature of the corrugated substrate potential. Therefore, measuring the PDSs yields important information on the intercalate–intercalate in-plane interaction as well as on the strength of the substrate potential.

5.1. In-plane PDSs in stage 1 alkali-metal compounds

Experimental results of PDS measurements for the alkali-metal in-plane modes in the stage 1 compounds IC_8 (I = K, Rb, Cs) are shown in figure 8. In the energy region scanned,

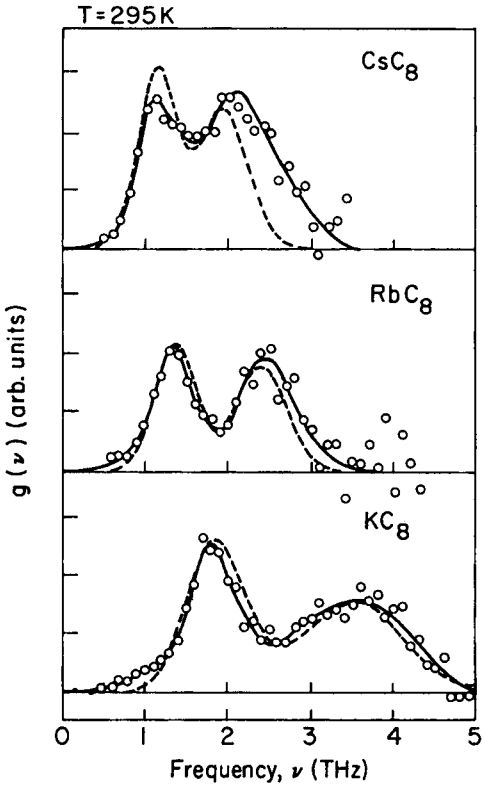

Figure 8. Measured PDSs of alkali-metal in-plane modes in stage 1 compounds. The broken curves are derived from a Coulomb force model. The model spectra have been braodened to take instrumental resolution effects into account. The full curves are guides to the eye (from [11, 12]).

the corresponding PDSs of the graphite host do not have any characteristic feature and are expected to contribute only to a gentle sloping background intensity. The partial PDSs of the alkali-metal in-plane modes consistently show a double-peak structure of about equal intensity, and the positions of both peaks scale roughly with the square root of the intercalate mass. Although such a shape of the PDSs is expected for a two-dimensional solid interacting with a substrate potential as discussed above, Kamitakahara *et al* [12] show that a simple BvK model is inappropriate for modelling the measured PDSs of alkali-metal GICs. A much better description of the observed PDS was achieved by a model in which the metal–substrate interaction is retained and described by a frequency ν_0. However, the alkali–alkali in-plane interaction is replaced by a long-range Coulomb interaction between the bare M^+ ions. In the absence of the I–C interaction the Coulomb model predicts that the upper peak occurs very close to the plasma frequency $\nu_p = e/(\pi M_I V)^{1/2}$, where V is the volume per M^+ ion. Turning on the substrate potential a frequency $\nu_c = (\nu_0^2 + \nu_p^2)^{1/2}$ is predicted for the upper peak. The calculated spectra for all three stage 1 compounds based on the Coulomb model are shown in figure 8 by the broken curves. The only fit parameter, ν_0, is chosen slightly below the frequency of the lower peak. This small shift is due to the weak alkali–alkali in-plane shear interaction. The calculated spectra have been broadened to take instrumental resolution and anharmonicity effects into account, and in particular for KC_8 and RbC_8 they reproduce the measurements rather well.

Another interesting feature of the Coulomb model is the fact that no conduction electron screening is required for the prediction of the upper phonon frequency. This implies that the conduction electron screening for small wavenumbers must be ineffective, i.e. the screening length of the conduction electrons must be larger than typical I–I atomic distances in the intercalate layer.

5.2. Stage 2 alkali-metal compounds

Stage 2 compounds differ from stage 1 compounds in many ways. The I–C interaction is weaker, the alkali-metal areal mass density is reduced and, in most cases, the alkali-metal layers form incommensurate modulated structures which melt at low temperatures. The intercalate in-plane modes are expected to be a sensitive probe of the discommensuration domain structure and of the melting transition. For instance, the first peak which is proportional to the strength of the I–C in-plane interaction should depend crucially on the location of the intercalate atom with respect to the substrate.

In the ordered low-temperature state a two-peak structure is again observed in the PDS, similar to the results on the stage 1 compounds. This is shown for KC_{24} in figure 9 [11]. In the low-temperature phase below 123 K, the lower frequency peak is surprisingly well defined, in spite of the fact that many of the alkali-metal atoms in the discommensuration domain structure do not sit precisely on commensurate sites with respect to the graphite substrate, and therefore should experience a distribution of I–C interactions. Upon heating above the melting temperature some anharmonicity becomes noticeable, but nothing dramatic takes place with increasing temperature in excess of T_c.

The observed shape of the PDS above T_c is fundamentally different from the expected one either for a simple liquid or a glassy state. In the first case, diffusive motion and vibrational excitation become indistinguishable in a region of phonon wavevectors probed there, leading to a broad quasi-elastic line shape of the dynamical scattering function centred at $\nu = 0$ [13]. In the second case, rather ill defined phonon excitations may exist as known for glassy metals [14], along with a resolution-limited central peak. In the present case, however, both types of excitations coexist, solid-like vibrational as well as liquid-like diffusional. The diffusional part, giving rise to a quasi-elastic peak, cannot be seen with the limited instrumental resolution of the triple-axis spectrometer using thermal neutrons but was unravelled using higher resolution time-of-flight spectrometer [15]. The phonon results discussed here indicate that the I–C in-plane interaction responsible for the lower peak in the PDSs remains important above T and that collective excitations giving rise to the upper peak persist upon melting. The fact that these solid-like features can coexist with liquid-like diffusional dynamics was interpreted as a strong signature for a two-dimensional melting process of a discommensuration domain structure which does not proceed through a transition of first order, but gradually transforms into a liquid by unpinning of domain walls via diffusive motion of atoms next to the domain walls [16]. At the same time, atoms that are located closer to the centre of domains are structurally more commensurate and give rise to phonon-like excitations. Finally, at high enough temperatures the alkali-metal layers become rotationally isotropic two-dimensional liquid when all atoms within the domains take part in the diffusion process. This view has recently been confirmed through molecular dynamics calculations (MDCs) by Fan *et al* [17].

Although the above discussion of the intercalate in-plane modes appears reasonable, recent analysis by Seong and Mahanti [18] show that the peak structure in the PDS requires a different interpretation. They performed MDC simulations and evaluated the partial PDS of the intercalant modes in stage 2 RbC_24. Based on these studies they argue that the double-peak structure is hidden within the first experimental peak and cannot be resolved because of the

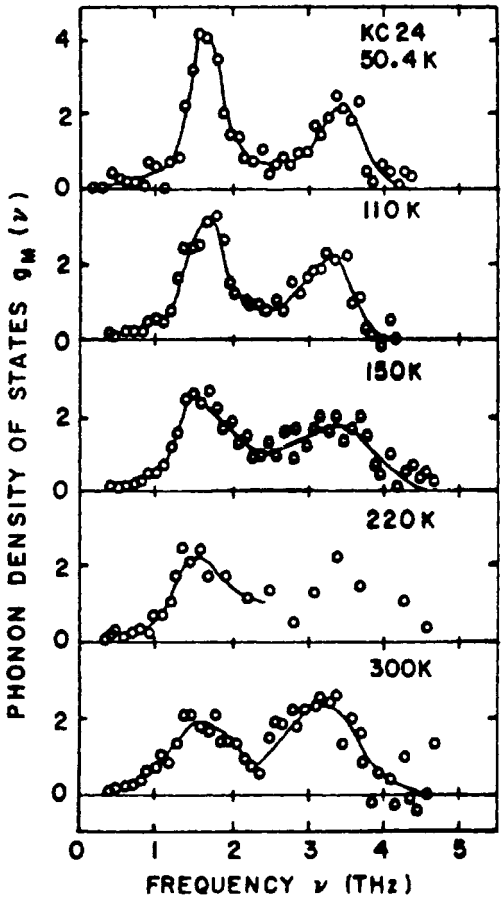

Figure 9. PDSs of intercalate in-plane vibrations in stage 2 RbK_{24} below and above the temperature for the discommensuration domain transition at 123 K (from [11]).

instrumental resolution. The high-frequency peak is attributed to two effects: (1) multiphonon corrections and (2) intercalant dynamics perpendicular to the graphite planes. Seong and Mahanti also calculated the PDS assuming a repulsive screened Coulomb interaction and comparing the results for the presence and absence of a graphite corrugation potential. Turning off the substrate potential results in a broad distribution of the PDS lacking the double-peak feature. Thus the strong substrate potential is essential for the observation of well defined intercalant in-plane modes at low frequencies as well as for a multiphonon peak at higher frequencies.

6. Conclusions

Layered structures and compounds offer an unusually rich variety of phonon modes. Unlike the lattice dynamics of isotropic crystals, the phonon branches in these highly anisotropic materials can be clearly separated in intralayer and interlayer modes, the energy separation between both being a direct measure of the anisotropy of the interatomic potentials. While normally the phonon branches extend over an energy range of about 0–60 meV, the low lying

phonon modes of graphite intercalation compounds terminate at about 25 meV, whereas the high-energy modes go up to 200 meV. Using inelastic neutron scattering much of the interlayer modes in layered compounds has been unravelled in the past. However, neutron scattering is limited to the lower lying modes and the cross over from collective layer-like modes to the intralayer modes cannot be studied. This gap could be closed using ultra-high-resolution inelastic x-ray scattering with synchrotron radiation. Promising first experiments have been carried out by Burkel *et al* [19], studying the top optic mode of graphite.

Acknowledgments

This work was supported by the Deutsche Forschungsgemeinschaft through the SFB 491 ('Magnetische Heteroschichten: Struktur und elektronischer Transport') and by the Ministerium für Wissenschaft und Forschung NRW, Germany.

References

[1] Zabel H and Solin S A (eds) 1990 *Graphite Intercalation Compounds I: Structure and Dynamics (Springer Series in Materials Science, vol 14)* (Berlin: Springer)
Zabel H and Solin S A (eds) 1992 *Graphite Intercalation Compounds II: Transport and Electronic Properties (Springer Series in Materials Science, vol 18)* (Berlin: Springer)
[2] Zabel H 1990 *Graphite Intercalation Compounds I (Springer Series in Materials Science vol 14)* ed H Zabel and S A Solin (Berlin: Springer) p 101
[3] Zabel H and Magerl A 1982 *Phys. Rev.* B **25** 2463
[4] Funahashi S and Kondow T 1983 *Synth. Met.* **6** 101
[5] Magerl A and Zabel H 1981 *Physics of Intercalation Compounds (Springer Series in Solid State Sciences)* ed L Pietronero and E Tosatti (Berlin: Springer) p 180
[6] Nicklow R M, Wakayabashi N and Smith H G 1972 *Phys. Rev.* B **5** 4951
[7] Wakayabashi N and Nicklow R M 1979 *Electrons and Phonons in Layered Crystal Structures* ed T J Wieting and M Schlüter (Dordrecht: Reidel) pp 409–64
[8] Kamitakahara W A, Wada N, Solin S A and Seaverson L M 1983 *Phys. Rev.* B **28** 3457
[9] Zabel H, Kamitakahara W A and Nicklow R M 1982 *Phys. Rev.* B **26** 5919
[10] Marshall W and Lovesey W 1971 *Theory of Thermal Neutron Scattering* (London: Oxford University Press)
[11] Kamitakahara W A and Zabel H 1985 *Phys. Rev.* B **32** 7817
[12] Kamitakahara W A, Wada N and Solin S A 1982 *Solid State Commun.* **44** 297
[13] Copley J R D and Rowe J M 1974 *Phys. Rev.* A **9** 1656
[14] Suck J B, Rudin H, Güntherodt H J and Beck H 1983 *Phys. Rev. Lett.* **50** 49
[15] Zabel H, Magerl A, Dianoux A J and Rush J J 1983 *Phys. Rev. Lett.* **50** 2094
[16] Zabel H, Hardcastle S E, Neumann D A, Suzuki M and Magerl A 1986 *Phys. Rev. Lett.* **57** 2041
[17] Fan J D, Reiter G and Moss S C 1990 *Phys. Rev. Lett.* **64** 188
[18] Seong H and Mahanti S D 1994 *Phys. Rev.* B **49** 5042
[19] Burkel E, Peisl J and Dorner B 1987 *Europhys. Lett.* **3** 957